ELSEVIER

Journal of Wind Engineering
and Industrial Aerodynamics 69–71 (1997) 239–248

JOURNAL OF
wind engineering
AND
industrial
aerodynamics

Computation of unsteady flow over a half-cylinder close to a moving wall

Sanjay Kumarasamy, Jewel B. Barlow*

University of Maryland, College Park, MD 20742-3215, USA

Abstract

Time-dependent Reynolds-averaged Navier–Stokes (RANS) simulations were performed for the flow over a half cylinder close to a moving wall. The gap between the cylinder and the moving wall was varied till the periodic shedding vanished. The resulting features are compared to the stationary wall case. When a vortex is shed from the edge closer to the wall, vorticity of opposite strength gets induced on the wall. The strength of this vortex depends on the kinematic condition on the wall. However, the gross flow characteristics, like the variation of Strouhal number, force coefficients and the base pressure with the gap ratios, are not affected much by the change in the kinematic condition.

1. Introduction

Flow over a bluff body exhibits an entire spectrum of flow features and continuing interest in this area makes it clear that the issues are far from resolved. Bluff body flows are characterized by large separated regions called wakes. In many engineering problems a wake is often in close proximity to a plane boundary or to other wakes. Practical examples abound in different areas of engineering. Automobiles, pipelines near sea bottom, and heat exchangers are some of them. Automobile flows are subjected to a different kinematic boundary condition on the wall, since the wall is often moving at the same velocity as the free stream. The interaction of the wake and the wall poses different and unique problems.

One approach to predicting the flow around complex shapes is to understand the flow physics for simpler cases and seek analogous features. Flows around two-dimensional bluff cylinders in ground effect, share many of these flow characteristics. For the flow around a two-dimensional bluff body, the instability of the shear layers leads to vortex shedding at most Reynolds numbers [1]. As the bluff body is brought

* Corresponding author.

PII S0167-6105(97)00158-X

into close proximity with a wall, it may be expected that the vortex shedding will be affected in some way since a bluff body attached to a plane wall does not show a strong periodicity. The gap at which periodic shedding vanishes, termed the critical gap ratio, depends on the shape of the body. Bearman and Zdravkovich [2] found that the critical gap for a circular cylinder is 0.3 times the diameter. Everitt [3] reported for a flat plate that the critical gap ratio was 0.5 and Kamemoto et al. [4] found for triangular cylinders the critical gap ratio to be 0.35. Taniguchi and Miyakoshi [5] were able to demonstrate a good correlation between the critical gap ratio and the boundary layer thickness for the case of a circular cylinder. To sum up, the flows on which previous reports are available are situations in which the shedding involves separation points which are not known a priori, e.g. circular cylinders or there is a subsequent shear layer interaction with the body e.g. rectangular cylinders.

The flow around a half cylinder in proximity to a plane wall, differs obviously from the circular cylinder. The separation points are fixed and are known a priori and the flow is smooth and attached to the body prior to the separation points. This important difference precludes one degree of freedom for the flow. The periodic shedding or the lack of it behind the half cylinder in and out of close proximity to the wall, hence, is of fundamental importance in under-standing two-dimensional separation and the stability associated with parallel shedding. Kumarasamy and Barlow [6–8] report that the critical gap ratio for the half cylinder close to a stationary wall is $0.33D$, and is large compared to the boundary layer thickness. It is expected that the boundary layer thickness on the wall with model in place will be considerably different compared to the case when the model is absent. In the extreme case of the moving wall, the classical boundary layer is completely absent although there is a non-zero gradient of the tangential velocity normal to the wall in the vicinity of the body due to the presence of the body. Hence, it is expected that the interference of the wall due to the presence of the boundary layer will be largely absent. The present study focuses on numerical computations for the half cylinder close to a moving wall with the aim of comparing the flow features of the stationary and moving wall results.

In the present work, a base line study is established by comparison of the results for the flow over the half cylinder in free stream. Grid dependence studies are performed for this case and the numerical accuracy with respect to the experimental simulations are ascertained. Then the effect of the wall is studied by changing the gap ratios. It is expected that the variation of the gross flow characteristics like Strouhal number and force coefficients will reveals the effect of the moving wall.

2. Numerical method

Computations were performed by solving the two-dimensional Reynolds-averaged Navier–Stokes equations,

$$\frac{\partial U_i}{\partial x_i} = 0; \quad \frac{\partial U_i}{\partial t} + U_j \frac{\partial U_i}{\partial x_i} + \frac{\partial P}{\partial x_i} - \frac{1}{\mathrm{Re}} \frac{\partial^2 U_i}{\partial x_j \partial x_j} + \frac{\partial}{\partial x_j} \overline{(u_i u_j)} = 0, \tag{1}$$

where U_i, $\overline{(u_i u_j)}$, and P represent the Cartesian mean velocities, Reynolds stresses, and pressure, respectively, and repeated indices indicate summation. For a successful RANS simulation one needs a good numerical scheme, consistent boundary conditions, high accuracy and an established turbulence model. In the present work, the equations are solved using the finite analytic technique (FA) [9–12]. The FA method decomposes the total region into a number of small elements in which local analytic solutions are obtained by local linearization. When the local analytic solution is evaluated at an interior node, it gives an algebraic equation relating the evaluated interior nodal value of its neighboring nodal values. The numerical solution of the total problem is then achieved by assembling and overlapping all local solutions. The finite analytic method thus differs from the finite difference and finite element methods in that the approximate algebraic analogy of the governing equation is obtained from an analytic solution. The scheme is formally second order accurate in space and first order accurate in time.

The problem of closure and the methods to overcome it, still remain a issues of paramount concern for RANS simulations and almost always represent the weakest link of all. The two-equation turbulence models employing turbulence kinetic energy and its dissipation rate, namely the k–ε turbulence model is popular in the engineering community. However, the standard k–ε model is not asymptotically consistent at all the wall and there is no natural boundary condition for the dissipation rate at the boundary. Hence, the inner layer is often computed by a different method, e.g. law of the wall, wall functions or a model based on single length scale. In the present work, closure is accomplished by employing a one-equation k–l for the near wall viscous sublayer and the standard k–ε model for the rest of the domain with the production term for the turbulence dissipation split into solenoidal and irrotational strains [13]. Bosch and Rodi [14] reported that the standard k–ε model coupled does not produce shedding below a gap ratio of 0.5 for the square cylinder while the experiments showed shedding well below that value. They have reported that by suitable modification for the turbulence production term they were able to capture the shedding. Present simulation aided by the modification mentioned above does predict shedding though below the experimental values.

3. Configuration and boundary conditions

3.1. Configurations

The vertical distance from the bottom edge of the cylinder to the wall non-dimensionalized by base diameter, Fig. 1, is defined as the gap ratio. The computational domain extends 10 diameters upstream, 15 diameters downstream and the top boundary is 8 diameters away from the body. Boundary layer spacing based on a Reynolds number of half a million, was used normal to the body. Grid density was made high in the wake region to adequately resolve the vortices. Fig. 2 shows the grid topology for a gap ratio of 1.583. There are 10 blocks and approximately 30 000 points in the domain. There is no explicit stability requirement akin to CFL number in the

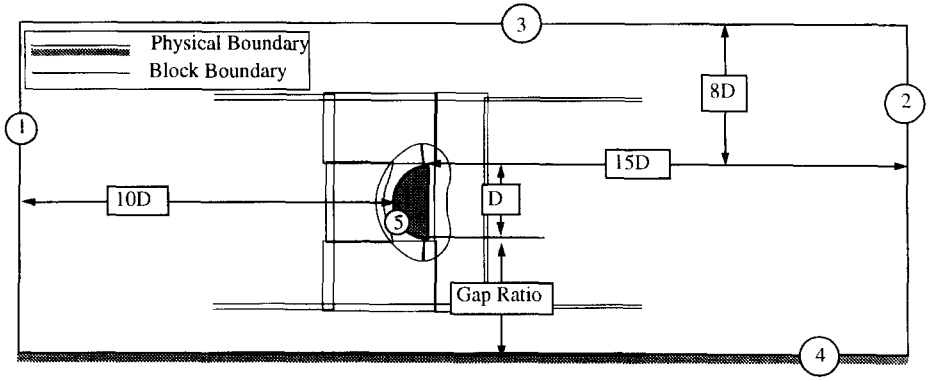

Fig. 1. Grid topology for gap ratio of 1.583.

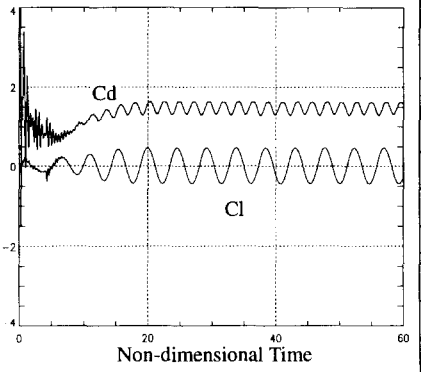

GR	1/GR	Strouhal Number		
		Static	Mov.	Expt.
Free	0.000	0.200		0.245
1.583	0.632	0.217	0.230	0.252
0.500	2.000	0.218	0.234	0.259
0.416	2.404	0.207	0.234	0.259
0.333	3.000	0.208	0.234	0.259
0.292	3.424	0.199	0.199	---
0.250	4.000	0.201	0.213	---
0.167	5.988	---	---	---

Fig. 2. Force coefficient variation.

finite analytic technique. The largest non-dimensional time step which lead to stable computation was 5×10^{-3}. This value is an order of magnitude smaller than the sampling rate needed to capture the shedding.

3.2. *Boundary conditions*

Various physical boundaries in the computational domain are numbered, and are shown in Fig. 1. The blocks have interior or overlapping boundaries which are only shown close to the body for clarity. A set of boundary conditions with U-velocity defined parallel to the X-axis and V-velocity defined parallel to Y-axis set of values of 1.0 and 0.0, respectively, pressure being extrapolated from the interior and turbulence quantities set to small free stream values, is collectively called the far-field boundary conditions. Boundaries 1 and 3 were implemented with a far-field boundary

condition. The far-field boundary 3 was extended to $12D$ for the free stream case to ascertain the sensitivity of the boundary location. The difference in the results were less than 5% when compared to the boundary at $8D$. The results reported below correspond to the second case where the boundary 3 is located at $8D$. Conditions on boundary 5, correspond to "no-slip" with U and V components of velocity set to 0.0, pressure was extrapolated from the interior and turbulence quantities are set to zero. Boundary 4 is similar to boundary 3 but "no-slip" here refers to the wall moving with the free stream velocity. Hence, the conditions are same as on boundary 5 except that U is set to a value of 1.0. The outflow boundary condition usually is implemented as the normal gradient of the flow variables set to zero. This condition is appropriate for steady-state flows or those flows which eventually reach a steady state solution. However, for periodic flow, which includes some of the cases here, this type boundary condition causes distortion of vortices which are convected out of the domain. It also caused a small reflection which was observed as a long period oscillation superposed on the time histories of force coefficients. The period correlated to the length of the domain downstream of the model. For these reasons, an open outflow boundary, namely a radiation boundary condition [15], was applied. This condition allows the large scale structures created within the computational domain to leave smoothly without reflection at the exit boundary. The open boundary condition is based on the Sommerfeld radiation condition, $\partial\varphi/\partial t + c\partial\varphi/\partial x = 0$ where φ is any dependent variable like u, v or p and c is the local wave speed ($c \geqslant 0$) which is calculated from the values ahead of the boundary using the results from the present time step and the previous one. Turbulence quantities were extrapolated at the exit boundary. The results showed marked improvement in the structures of the vorticity, and the long period oscillation was removed.

4. Results

4.1. Computations

For the steady flow, the flow variables are usually stored after the solution is converged. In time-dependent flow simulations like the present one, some of the salient features of the flow like the force coefficients were recorded at each time step. Pressures on the body and on the wall were stored every 20 time steps. The force coefficients are obtained from the integration of the pressures and shear stresses on the body. Strouhal number is defined as $\mathrm{St} = fD/U$ where the frequency is obtained from the time history of the force coefficients. Reynolds number based on the diameter of the cylinder was 468 000. The gap ratios chosen were: infinity which corresponds to free stream, 1.583, 0.50, 0.416, 0.333, 0.292, 0.250 and 0.167. All the simulations were performed till there were at least 20 cycles of the dominant shedding frequency. Since the main motivation of the study is to capture the vanishing of shedding, no explicit triggering was performed initially. It took at least 6000 times steps to come to a stationary state. The Reynolds number and the gap ratios were chosen so that direct

comparison with the stationary wall results, both experimental and computational, could be preformed.

4.2. Free stream

The grid topology for the free stream case consists of an "O"-type grid wrapped around the body with the other blocks begin rectangular. Necessary overlaps are provided for data communication. The grid consists of 10 blocks with a total of 30 000 grid points and was made symmetrical about the X-axis so that there is no grid basis to influence the shedding to be non-symmetrical. The corners on the top and the bottom edges have been rounded of with a radius of 0.001 and the included angle is less than 0.2°. Fig. 2 shows the variations of lift and drag coefficients. As was noted earlier, no explicit triggering was provided and the flow naturally develops into alternate shedding. From Fig. 2 it can be observed, as previously noted, that it takes at least 6000 timesteps (corresponding to non-dimensional time of 20) for the stationary state to be reached. C_l exhibits a sinusoidal variation corresponding to a Strouhal number of 0.2. This reasonably agrees with the experimental value of 0.245. For every lift cycle, drag undergoes two cycles since the effect of each vortex shed from the top and bottom edges are the same on drag whereas the vortices shed from top and bottom induce life of opposite signs. Hence, it is expected that the drag should vary at twice the Strouhal number corresponding to lift. The time-averaged lift coefficient is zero which suggests that the effect of vortices shed from either edge on the lift variation is antisymmetric. The maximum and minimum values are 0.5 to -0.5. The mean value of drag without including the initial transients, is 1.5. Closer inspection of the drag coefficient variation reveals a small plateau at the extremes and a small cycle to cycle variation [16].

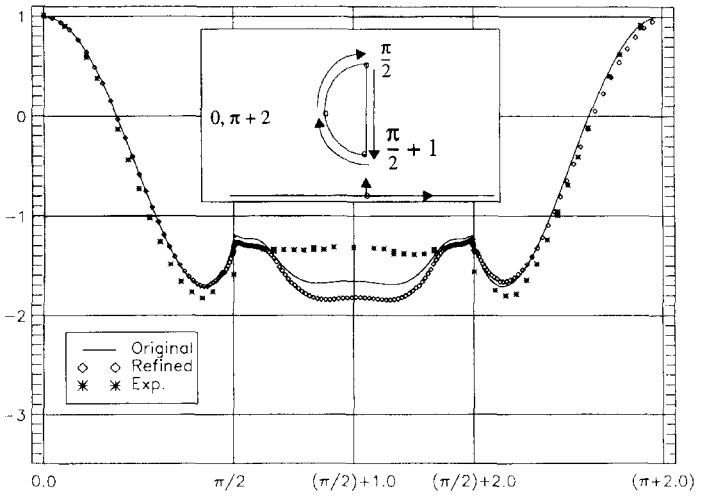

Fig. 3. C_p (average) distribution – free stream.

The time-averaged coefficient of pressure (C_p) distribution is as shown in Fig. 3 along with the convention for the abscissa. The plot compares three results, namely, the experimental values and the computational values for two grids. The coarse grid and the refined gird shows some difference in the base region. The refined grid was obtained by decreasing the vertical spacing in the wake substantially and the details of the distribution of the point density is given in Ref. [17]. The pressures match with the experimental values till the separation point and even the peaks are captured quite accurately. Base pressure though shows a significant difference in values between the experiment and computations. Also, the distribution of the pressure on the base is quite flat. Similar results were observed for the flat plate, though much pronounced and at much smaller Reynolds number by Roshko [18]. It is the authors conclusion that the limitations of the turbulence modeling is the primary cause for the poor agreement in the base region. Three dimensionality is a potential candidate too. Since refined the grid did not improve the comparison, it was decided to use the coarse grid for the subsequent studies. The free stream case establishes the baseline study for the current computation with its accuracy identified by comparison to the experimental results.

4.3. Ground effect

4.3.1. Strouhal number

The grid was minimally modified for the presence of the wall. The Strouhal number for various gap ratios are summarized in Table 1. Experimental Strouhal numbers were obtained from the signal measured by the transducers placed on the edges of the cylinder, corresponding to locations $\pi/2$ and $2 + \pi/2$. Refer to Fig. 3 for the coordinate convention. The Strouhal number does not show much variation with gap ratio. The same observations were reported by Bearman [2] though Angrilli et al. [19] report a slight increase in the Strouhal number for circular cylinders.

4.3.2. Variation of force coefficients

Fig. 4 shows the variations of lift and drag coefficients plotted as a function of the inverse of the gap ratio so that the free stream value corresponding to a gap ratio of infinity can be represented easily. Experimental results correspond to the stationary wall case and the force coefficients for the experiments were evaluated from the integration of the mean pressure distribution around the body [6]. Since the aerodynamic forces for this particular body shape are dominated by the pressures and relatively little affected by the shear stresses, it is expected that these would be representative of the total values. Computational results were also obtained from the integration of the mean pressures around the body so that a consistent comparison can be made. Mean lift coefficients increase from zero to about 0.8 as the gap ratio is decreased. Computational values are in excellent agreement with the experiments and there is only a small difference between the stationary wall and the moving wall cases. Drag does not compare well with the experimental values due to the underprediction of the base pressure. Moving wall drag coefficients differ from the stationary wall values and they are not evenly distributed about the stationary wall case.

4.3.3. Flow features

When the gap ratio is decreased it is expected that the boundary layer on the wall and the shedding will interact. In the case of the stationary wall, the boundary layer on the wall supports and aids the induction of the vorticity of opposite strength whenever the vortex from the bottom edge forms. The contour plots, Fig. 5, show the time-averaged value of the vorticity instead of frozen time shots at various time levels to reduce the number of figures. The time-averaged contours are obtained by the averaging the computational results over an entire shedding cycle. The secondary vortex grows and gains in strength as the primary vortex from the bottom edge develops. Latter it erupts from the wall and gets convected downstream. The presence of the stationary wall significantly alters the trajectory of the shed vortices. In the case of the moving wall, due to the absence of the classical boundary layer on the wall, the secondary vortex strength is greatly reduced though not eliminated. Also, the shed vortices convect much closer to the wall. It is important to note that the significant changes in the flow field occur entirely downstream of the body. Since the drag

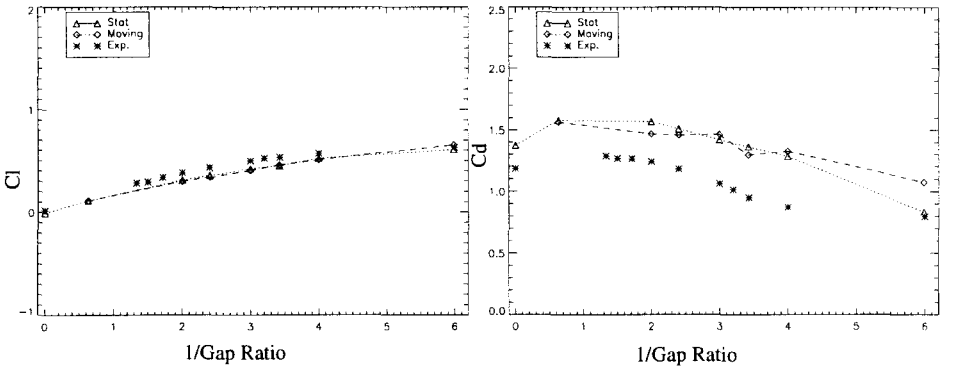

Fig. 4. Variation of force coefficients with gap ratio.

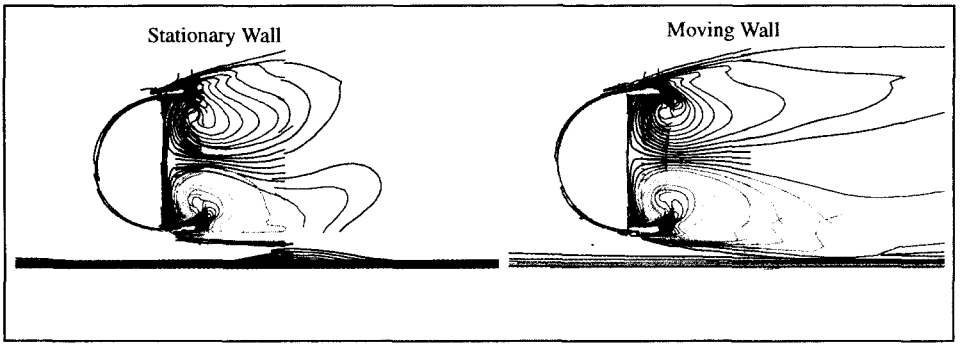

Fig. 5. Vorticity contours of the mean flow.

contribution mainly comes from the base region, the change in the kinematic condition on the wall affects only indirectly the base pressure by the presence or the absence of the secondary vortex.

5. Conclusions

Flow over a half cylinder in close proximity to a moving ground is computationally simulated by solving the RANS equations in time accurate fashion. The computational results are compared to the flow over the half cylinder in close proximity to a stationary wall. From the results presented the following conclusions are drawn:

The Strouhal number associated with the primary shedding frequency did not change due to the moving wall. The critical gap ratio, defined as the maximum gap ratio below which there is no organized shedding, was not affected either. Variation on the Strouhal number with respect to the gap ratio is small, similar to the stationary wall. Vorticity formation and shedding phenomena are little affected by the kinematic condition on the ground. This is further collaborated from the flow pictures which show that even in the stationary case the boundary layer thickness gets reduced due to the local acceleration of the flow and there is a potential region between the body and the wall. This potential core region acts as a buffer zone preventing the boundary layer from directly interacting with the vortex formation. In the case of the moving wall, this region is more pronounced.

There is no variation in the lift coefficient between the stationary and moving wall cases. This is due to the fact that lift comes entirely from the region upstream of the base. As pointed out earlier, there is little change in the flow features close to the body, upstream of the base region. The presence of the potential region in the gap dampens the effect of the wall condition and hence does not produce a change in the pressure distribution on the front surface of the body. However, the drag shows a large deviation from the stationary wall case. It is due to the presence or absence of the secondary vortex downstream of the body which changes the trajectory of the vortices shed. From the mean flow concepts [18], the wake curvature will affect the base pressure which affects the drag force. At a gap ratio of 0.167, below the critical gap ratio, the drag corresponding to the moving wall is substantially more than the stationary wall due to the differences in base pressures.

In conclusion, it is observed that the nature of the kinematic condition did not change the gross characteristics of the flow. The difference is drag values is related to the difference in the base pressures and is due to the presence or absence of secondary vortex. Hence, the effect of the wall is indirectly felt. Two important issues needs to be further investigated. First, the comparison of the moving wall computations to the experimental values. Though the confidence level in predicting the lift, Strouhal number, and in general the trends is high with the computational solutions, existence of the experimental results would be helpful because of the complex nature of the flows. Unfortunately, experimental moving wall simulations are neither easy nor cheap. However, boundary layer control by wall jet blowing is one potential method that might be used effectively. Second, the nature of the boundary condition has the

least effect on the critical gap ratio. If there is a potential region between the body and the wall, the vanishing might be due to inviscid instability as described in Ref. [6].

References

[1] H. Lamb, Hydrodynamics, Dover, New York, 1932.
[2] P.W. Bearman, M.M. Zdravkovich, Flow around a circular cylinder near a plane boundary, J. Fluid Mech. 89 (1978) 33–47.
[3] K.W. Everitt, A normal flat plate close to a large plane surface, Aerodyn. Quality 33 (1982) 90–103.
[4] K. Kamemoto, Y. Oda, M. Aizawa, Characteristics of the flow around a bluff body near a plane surface, Bull. JSME 27 (230) (1984).
[5] S. Taniguchi, K. Miyakoshi, Fluctuating fluid forces acting on a circular cylinder and interference with a plane wall, Exp. Fluids 9 (1990) 197–204.
[6] S. Kumarasamy, J.B. Barlow, Interference of plane wall on periodic shedding behind a half cylinder, AIAA-Paper 95-2285, 1995.
[7] S. Kumarasamy, J.B. Barlow, Unsteady flow over a bluff body adjacent to a plane wall, CFD-16 Open Forum 12th AIAA Computational Fluid Dynamics Conf. San Diego, 1995.
[8] S. Kumarasamy, J.B. Barlow, Unsteady flow over a bluff body adjacent to a plane wall, 14th AIAA Applied Aerodynamics Conf., New Orleans, 1996.
[9] H.C. Chen, V.C. Patel, S. Ju, Solutions of Reynolds-averaged Navier–Stokes equations for three-dimensional incompressible flows, J. Comput. Phys. 88 (1990) 305–336.
[10] C.J. Chen, Handbook of Numerical Heat Transfer, Wiley, New York.
[11] K.M. Weems, R.A. Korpus, Users Manual for the SAIC Finite Analytic Navier–Stokes Code SAIC, Marine Hydrodynamics Division, Annapolis, MD, 1992.
[12] H.C. Chen, R.A. Korpus, A multiblock finite-analytic Reynolds-averaged Navier–Stokes methods for 3D incompressible flow, ASME Summer Fluid Dynamic Confer., 1993.
[13] K. Hanjalic, B.E. Launder, Sensitizing the dissipation equation to irrotational strains, Trans. ASME 102 (1980).
[14] G. Bosch, W. Rodi, Simulation of vortex shedding past a square cylinder near a wall, Proc. 10th Turbulent shear Flow Symp., Penn State, 1995.
[15] T.Y. Han, J.C.S. Meng, G.E. Innis, An open boundary condition for incompressible stratified flows, J. Comput. Phys. 49 (1983) 276–297.
[16] S. Kumarasamy, J. Barlow, Computational aeroacoustics of the flow over a half cylinder, 34th Aerospace Sciences Meeting and Exhibit, Reno, 1996.
[17] S. Kumarasamy, Incompressible flow simulation over a half cylinder with results used to compute associated acoustic radiation, Ph.D. Thesis, Department of Aerospace Engineering University of Maryland, College Park, MD, 1995.
[18] A. Roshko, Perspectives on bluff body aerodynamics, J. Wind Eng. Ind. Aerodyn. 49 (1993) 79–100.
[19] F. Angrilli, S. Bergamaschi, V. Cossalter, Investigation of wall induced modifications to vortex shedding from a circular cylinder, Trans. ASME 104 (1982).